ADVANCED INTELLIGENT SYSTEMS
Open Access
www.advintellsyst.com

# Fused Deposition Modeling-Based 3D-Printed Electrical Interconnects and Circuits

*Habib Nassar and Ravinder Dahiya**

**Multimaterial 3D printing in electronics is expanding due to the ability to realize geometrically complex systems with simplified processes compared with conventional printed circuit board. Herein, the feasibility of using a copper-based filament to realize 3D circuits with planar and vertical interconnections is presented. The resistivity of the tracks (1–3 mm wide) is studied with reference to printing parameters and orientation. Using lateral infill for 1 mm tracks offers lower resistance compared with longitudinal infill (≈75%). For wider tracks, the effect of infill orientation on resistance diminishes. The evaluation of tracks embedded in polylactic acid shows a drop in maximum current (to ≈11 mA) compared with exposed tracks (≈16 mA). There is no observed correlation between electrical performance and number of embedding layers. However, a significant correlation is observed between the tracks' resistance and the amount of time the filament remains in the heated nozzle. This in-depth study leads to optimum resolution to realize conductive tracks of 0.67 mm thickness and the first integration of fused deposition modeling (FDM)-printed conductive traces with small-outline integrated circuits to open a pathway for higher-density 3D printed circuits. Finally, the transmission of digital data by a 3D printed circuit is demonstrated.**

## 1. Introduction

Smart structures and robust embedded systems are becoming prevalent in several fields, including biomedical instrumentation, robotics, prosthetics, and environmental monitoring.[1–5] This is particularly true for electromechanical devices offering sensory perception with local processing and intelligence.[6,7] Additive manufacturing (AM) or 3D printing is an attractive technique for the fabrication of such devices as it allows us to manufacture fully customizable devices with integrated electronic systems, thus simplifying supply chains and manufacturing processes. AM can also offer a pathway for less waste in the electronics industry with only the amount of material needed for the fabrication process used. Due to these features, 3D printing systems are constantly being advanced with the ability to print a wide range of functional materials needed to enable complex electronic and sensor structures.[8–10] In that direction, fully embedded, multipurpose, out-of-plane circuits by 3D printing could allow efficient use of 3D space in any given package.[11] In doing so, AM could also provide an attractive alternative for 2D printed circuit boards (PCBs), paving the way for the fabrication of 3D circuits and eliminating the chemical-heavy processes involved in standard PCB fabrication.[12,13] To achieve such electronic systems, it is important to equip 3D printers with multimaterial printing capabilities, that is, printing conductive materials and dielectrics.

The most common technique of multimaterial 3D printing for embedded electronic circuits is to combine one printing method with a direct ink write (DIW) setup that dispenses conductive inks. This has been demonstrated with stereolithography (SL),[14–23] fused deposition modeling (FDM),[11,24–30] ultrasonic additive manufacturing (UAM),[31] or DIW itself.[32–35] Among the different types of 3D printing techniques, FDM would provide the most widespread and readily achievable form of 3D circuits.[36] A combination of its affordability, open-source nature, and wide range of compatible materials makes it a great choice for the application of 3D-printed functional materials and embedded conductive interconnects. It also alleviates the need for high thermal curing and sintering temperatures, which are used to process some printed conductive inks. Basic circuits have been printed using conductive filaments and FDM but without much success in terms of characterizing electrical performance and optimization.[37–43] To achieve reliable 3D-printed electronic circuits, the fabricated parts require sufficient characterization, with specific emphasis needed on the electrical and thermal characterization of the materials used. Further, the issues such as the adhesion between materials, polymer melting temperatures, the accumulation of heat generated from the interconnects, etc. that can affect the electrical performance of thermoplastic conductive polymers embedded in nonconductive thermoplastic polymers have to be investigated. To our knowledge, the only study available on the

H. Nassar, R. Dahiya
Bendable Electronics and Sensing Technologies (BEST) Group
James Watt South Building, School of Engineering
University of Glasgow
Glasgow G12 8QQ, UK
E-mail: Ravinder.dahiya@glasgow.ac.UK

The ORCID identification number(s) for the author(s) of this article can be found under https://doi.org/10.1002/aisy.202100102.



**DOI: 10.1002/aisy.202100102**

effect of embedding on the electrical performance of interconnects is based on solid copper wires and not printed conductive materials.[44] Furthermore, there is still a knowledge gap in the optimization of FDM printer resolution for conductive materials and the integration of surface mount devices (SMDs). The optimization of printer parameters is possible through artificial intelligence and data-driven approaches.

This article assesses the feasibility of using FDM 3D printing as a method of embedded electrical interconnects from a copper-based conductive polymer composite. This is done by 1) evaluating the optimal printing conditions to achieve printed tracks with the highest conductivity and highest resolution; 2) understanding the effect of embedding both planar and vertical Electrifi interconnects in an insulating thermoplastic on their conductivity; 3) determining the effect of embedding on the electrical range of operation of the printed Electrifi tracks; and 4) analyzing the use of the printed conductive tracks in carrying digital signals from an integrated circuit (IC) using the interintegrated circuit ($I^2C$) communication protocol. From the available commercial conducive filaments, the Electrifi filament offers the highest conductivity and is therefore used in this study. A comparison is provided in Supporting Information.

## 2. Experimental Section

### 2.1. Materials and Printer Setup

The conductive polymer composite used in this study was the copper-based Electrifi filament (Multi3D LLC, USA). The substrate material used to embed the printed conductive interconnects was polylactic acid (PLA) (RS Components, UK). The printer used for fabricating the test structures and application circuit was the Ultimaker S5 printer (Ultimaker B.V, The Netherlands). Making use of the printer's multimaterial printing capacity, both the packaging and conductive materials were deposited in a single print run. **Figure 1**a shows a multinozzle FDM 3D printer and Figure 1b shows potential configuration of embedded FDM 3D circuits. Both print heads on the carriage were retractable, making it less likely that one nozzle negatively affected the print when the other was printing by scraping the top printed layer. A prime tower was printed at the edge of the build plate to ensure consistent flow through the nozzles before depositing further material on the printed part. The heated bed option in the printer was enabled to examine the effect of the printing environment on the electrical performance of the printed filaments. Finally, blue masking tape was used on top of the print bed to enhance the adhesion between the printed structures and the plate.

The computer-aided design (CAD) models were made using SolidWorks and the slicer software Cura was used to generate the g-code files for the printer. Retraction is an important property for multimaterial 3D printers as it helps to prevent oozing of one material during the printing of the second material. However, as with the Electrifi filament used in this article, some filaments might be too soft to handle repeated retraction moves. This is because the repeated moves might cause grinding of the filament at the extruder and hence, errors in the amount of material deposited through the nozzle. Therefore, prints were conducted with retraction disabled for Electrifi.

The Electrifi print speeds were limited to $10\,mm\,s^{-1}$ with some prints conducted at $5\,mm\ s^{-1}$. This is because when using softer and bendable filaments, lower print speeds are recommended for better print quality. The infill density was kept at

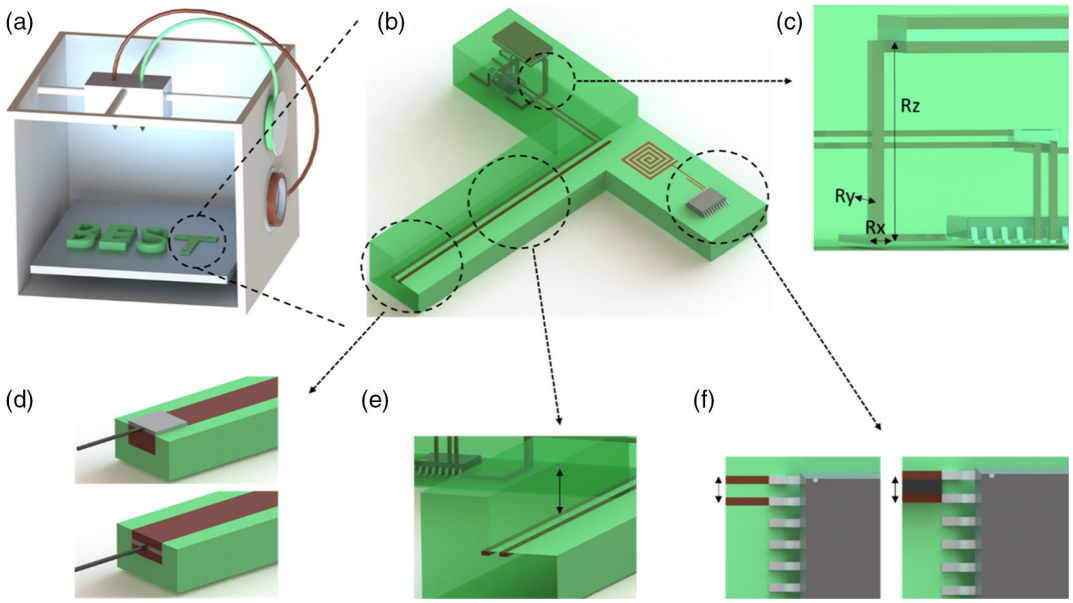


**Figure 1.** FDM 3D printing circuits using a a) multimaterial printer loaded with both substrate and conductive polymer composite filaments. b) Demonstration of a potential configuration of embedded FDM 3D circuits, sensors, and systems to explore c) electrical performance in the XYZ-axes, d) methods of reducing contact resistance with external wiring, e) effect of embedding on electrical performance and thermal durability of the conductive composites, and f) the achievable resolution for the integration of the printed interconnects and surface mount components with separation material.

100%, and the optimized wall printing order feature was enabled. These settings were used to ensure sufficient contact between the printed rasters of the conductive filament to maximize the achievable conductivity.

### 2.2. Printing Resolution and Dimensional Accuracy

Both 0.4- and 0.25 mm-diameter nozzles were used along with different print parameters to achieve the smallest reliable printed conductive interconnects with the Electrifi filament. For the 0.4 mm nozzle, Electrifi tracks with widths of 1, 0.8, 0.7, 0.6, 0.5, 0.45, and 0.4 mm were printed on the blue tape directly onto the print bed. Five tracks were printed for each width (Figure S3, Supporting Information). The print parameters used for each nozzle are shown in **Table 1**.

With the goal of embedding small-outline integrated circuit (SOIC)-packaged SMDs, the printed conductive interconnects should have a track width of 0.41 mm and a pitch of 1.27 mm. To this effect, a structure consisting of 14 conductive lines with 7 printed on either side of where the IC would be placed is designed and printed using the 0.25 mm nozzle (Figure 3c). The tracks are printed on the surface of the PLA substrate, extending on either side to contact pads for external connections. The conductive polymer composite tracks are printed directly on the surface of the substrate with PLA printed between them. The thin track of substrate material printed between the conductive tracks acts as both a separator to help prevent shorting of the conductive tracks and a base for further layers in the *Z*-axis when embedding components is needed. A similar structure is also printed with a track width of 0.2 mm and a pitch of 0.65 mm using 0.25 mm to test the limit of the nozzle (Figure S4, Supporting Information). The dimensions in the *X*- and *Y*-axes are observed through an optical microscope (Eclipse LV100NP, Nikon, Japan) fit with a camera (MC170 HD, Leica, Germany). The electrical continuity was tested using a multimeter touching the printed contact pads. The dimensional accuracy in the vertical *Z*-direction of the printer setup is evaluated by printing tracks on the blue tape directly on the print bed and measuring their thicknesses in the *Z*-direction using a profilometer (Veeco Dektak 6M Height Profiler, Bruker, USA). With the use of the 0.4 mm nozzle, Electrifi tracks with planar dimensions of 10 mm × 20 mm are printed with thicknesses of 300, 600, and 900 µm using the settings shown in Table 1 (apart from the layer height which is changed for this experiment). The layer heights used here are 0.1 and 0.3 mm.

**Table 1.** Print parameters for the planar resolution prints.

| Setting | 0.4 mm nozzle | 0.25 mm nozzle |
|---|---|---|
| Layer height [mm] | 0.3 | 0.1 |
| Line width [mm] | 0.35 | 0.23 |
| Wall line width [mm] | 0.4 | 0.23 |
| Print temperature [°C] | 150 | 150 |
| Flow [%] | 110 | 100 |
| Print speed [mm $s^{-1}$] | 10 | 10 |

### 2.3. Effect of Printing Orientation on the Conductivity

Based on a study conducted on the bonding quality of FDM-printed polymer parts, it has been reported that the orientation of printing could affect the porosity of the structure.[45] This is due to the time the heated nozzle spends near a location on the track and the average building temperature at that point over the print process. In this article, the effect of this phenomenon on the conductivity of the printed polymer composite is evaluated. Electrifi tracks are printed as channels on the PLA substrate with varying track widths of 1, 2, and 3 mm. Samples with both longitudinal and lateral infill orientations are printed (**Figure 2**). Five samples are printed for each infill orientation and track width combination. The effects of nozzle temperature, print bed temperature, track width, and nozzle diameter on the conductivity are also evaluated. Moreover, the best technique for reducing the contact resistance between the printed conductive tracks and external wiring is evaluated. These experiments and results are explained in the Supporting Information (Figure S1, S2, and S5, Supporting Information).

### 2.4. Electrical Characterization of the Embedded Tracks

The electrical characterization tests on the printed Electrifi tracks are split into three categories: 1) the effect of embedding in PLA on the conductivity of both planar and vertical tracks; 2) the effect of embedding in PLA on the DC electrical performance under an incremental current test; and 3) the effect of embedding in PLA on the DC electrical performance under a constant current stress test. The printing of the substrate and embedding materials affect their heat transfer capabilities by altering how localized Joule heating builds up at the conductive tracks depending on their mechanical properties and porosity.[46]

The first tests are conducted on both planar and vertical Electrifi tracks, and their resistance values are measured using a two-probe DC resistivity setup with an Agilent 34461 A digital multimeter (Keysight Technologies, Santa Rosa, CA, USA). The planar tracks are printed in two configurations both of which have dimensions of 30 mm × 1 mm × 0.6 mm. In the first configuration, the number of bottom PLA layers on which the Electrifi was printed onto is increased by 1 for every increase in the number of top embedding PLA layers (1−3 layers). In the second configuration, the number of bottom PLA layers

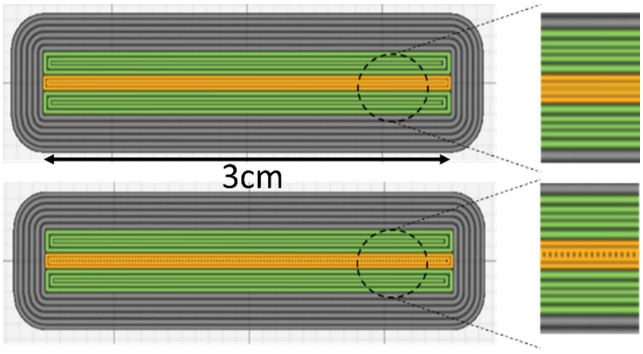


**Figure 2.** Top-layer view of the sliced prints with the conductive track in the middle showing longitudinal infill (top) and lateral infill (bottom).

remains constant and only the number of top embedding PLA layers increases (1−3 layers, constant substrate thickness). The vertical tracks are printed with dimensions of 2 mm × 2 mm × 10 mm. The vertical tracks are embedded in PLA substrate materials in all directions. The thickness of the embedding PLA is 1.5 mm on the sides and 0.2 mm on the top and bottom. Exposed versions of Electrifi of all the configurations are printed for comparison. The nozzle diameter, nozzle temperature, bed temperature, and layer height used are 0.25 mm, 150, 40 °C, and 0.2 mm, respectively.

The second tests are conducted on the planar, constant substrate thickness samples. A Keysight B2912A precision source measurement unit (SMU) (Keysight Technologies, Santa Rosa, CA, USA) is used to apply current to the printed tracks and measure the voltage across them. The current applied is 1 mA and is increased by 1 mA every 10 s until the conductive track fails. Failure, in this case, is defined as when the resistance of the track increases to more than double its original value.

In the third tests, a constant current is supplied through the printed planar, constant substrate thickness tracks, and the voltage across them is measured using the SMU. The current is supplied until failure. For both sets of electrical performance tests, an infrared (IR) thermometer is used to scan the top of the tracks at a fixed distance. This is to quantify the Joule heating in the tracks and correlate an increase in temperature with current- and voltage-carrying capabilities of the tracks. Five samples for each number of embedding layers are tested.

## 3. Results

### 3.1. Effect of Printing Conditions and Parameters on Resolution

The printed structure demonstrating the optimized resolution is shown in **Figure 3**a. A resolution high enough to be compatible with SOIC-packaged ICs is achieved. The average track width and gap width achieved with this design and using the 0.25 mm-diameter nozzle are ≈0.57 and ≈0.67 mm, respectively (**Figure** 3b and 4b). Designing and printing thinner tracks and smaller gaps resulted in filament spreading and undefined tracks. The low melting temperature of the filament as well as the overflow of material from the nozzle resulted in a covering of the nozzle tip with Electrifi material preventing well-defined tracks from being extruded from the nozzle (Figure S4, Supporting Information). The extrusion with the stepper motor feeder is not fine enough to produce consistently thinner tracks. Some solutions to this could be to use a base thermoplastic and composite with more favorable rheological behavior, print the thermoplastic with direct drive extrusion or in pellet form rather than with a Bowden tube, or further fine tune print parameters such as flow and extrusion multiplier. As for the gaps between the tracks, the printer's XY gantry and belt movement system is capable of a resolution of 6.9 µm. This provides a theoretical value for the achievable gap width very close to the nozzle diameter. However, the spread of the filament as it leaves the nozzle onto the print prevents consistently smaller gaps from being printed (<0.67 mm).

The minimum track width achieved with the 0.4 mm nozzle is ≈0.6 mm (Figure 4a). As the designed width decreases, so does the measured printed width. The measured width does not exactly match the designed width due to the presence of an offset caused by the spreading of the filament as it exits the nozzle. This decreases plateaus at 0.6 mm even when the designed width is <0.6 mm.

It is reported that the width of a printed track using FDM cannot be realized to be less than 1.2−1.5 times the width of the printer nozzle's diameter.[47] This is in part caused by the spreading of the filament as it leaves the nozzle and the stress it is under is relaxed, releasing elastically stored energy. Reducing the nozzle diameter will reduce the minimum feature size achievable. Nonetheless, the amount of pressure needed to extrude the polymer melt through the nozzle poses a limit to the decreased diameter size. This pressure drop ($\Delta P$) increases as the nozzle

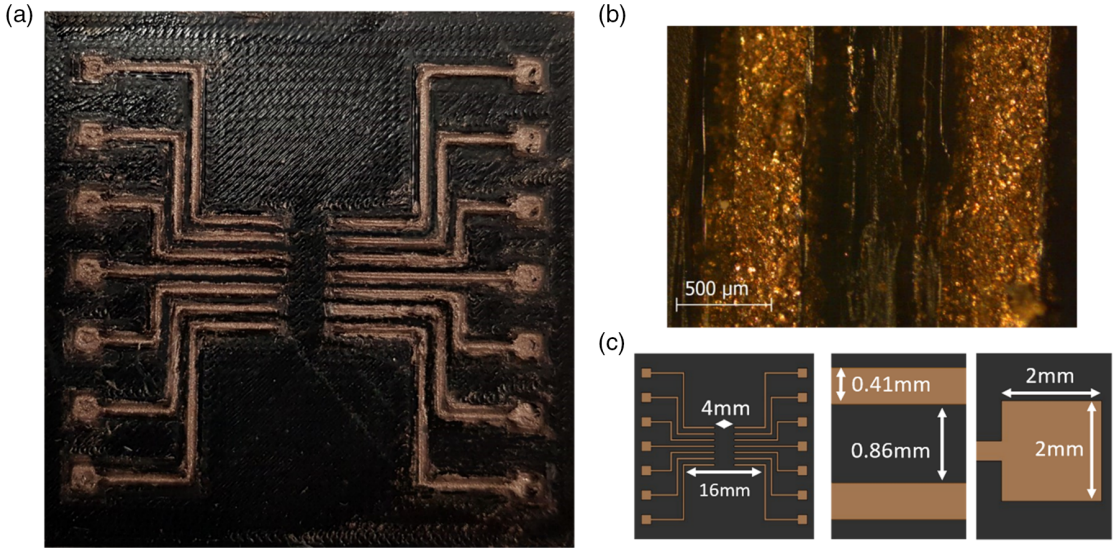


**Figure 3.** Dimensions of the planar resolution prints. a) Printed structure with optimized resolution for SOIC IC packages. b) Optical microscope image showing both track and gap width of the printed structure. c) The designed dimensions of the full structure, track widths, gap widths, and contact pads.

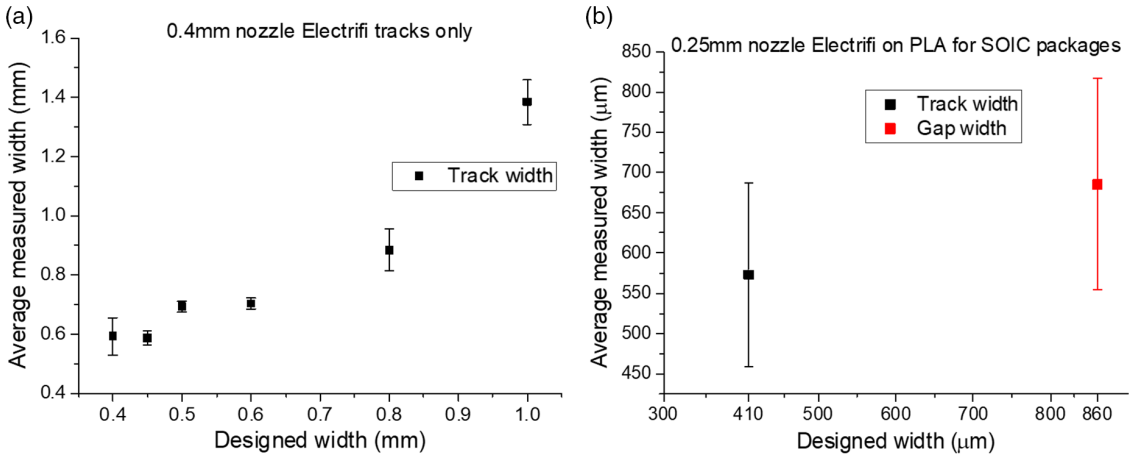


**Figure 4.** Designed width versus average measured width for a) Electrifi tracks on print bed with 0.4 mm nozzle and b) Electrifi tracks on PLA with 0.25 mm nozzle.

diameter decreases. The extruder stepper motors on the roller feed mechanism provide the necessary amount of force needed to overcome this drop in pressure. The amount of power that is required from the motor ($P_{mot}$) is calculated according to the following equation.[47,48]

$$P_{mot} = \frac{1}{2}\Delta P A \omega_r R_r \quad (1)$$

where $\omega_r$ is the angular velocity of the pinch rollers. $R_r$ refers to the radius of the pinch rollers, whereas $A$ is the filament's cross-sectional area. An absence of slip between the rollers and the filament is assumed. Another limit on the nozzle diameter is the pressure from the motor used to extrude the polymer melt through the nozzle. Above a certain pressure, the compression may induce buckling of the filament. The critical buckling pressure ($P_{cr}$) can be estimated using the following equation.[47,49,50]

$$P_{cr} = \frac{\pi^2 E d_f^2}{16 L_f^2} \quad (2)$$

where $E$ is the elastic modulus of the filament. The diameter of the filament is referred to by $d_f$, whereas $L_f$ refers to the length of the filament form the rollers to the nozzle liquefier. All these limitations are considered when evaluating the consistency of electrical performance between printed interconnects.

The choice of layer height is considered with regard to the relationship between layer height and nozzle diameter. As a rule of thumb, it is recommended to keep the layer height below 80% of the nozzle diameter.[51] Going higher than that could lead to the layers not bonding well to each other because the nozzle will not press the current layer against the previous one. Moreover, keeping the layer height above around 20% of the nozzle diameter helps avoid back pressure from the nozzle, which can cause inconsistent printing.[52] So, for 0.4 mm nozzles, the layer height should be between 0.08 and 0.32 mm, and for 0.25 mm nozzles, the layer height should be between 0.05 and 0.2 mm. This, however, will naturally give rise to a trade-off between the adhesion of layers, printing resolution, and the conductivity of polymer composite filaments, which have been shown to have higher conductivities when larger layer heights are used. Consistent thicknesses of printed tracks are needed for consistent electrical performance and resistance values. This is partly dictated by accurately printing tracks with the desired thickness and small variations between printed samples.

**Figure 5** shows the accuracy of the Ultimaker S5 printer in the vertical $Z$-axis. Printing at a 0.1 mm layer height produced both more accurate and more precise structure thicknesses than when printing with a 0.3 mm layer height. This shows that printing with a smaller layer height, or a layer height that is not near the boundary of recommended values for the nozzle diameter, produces more accurate thicknesses of Electrifi material. This allows consistent interconnect printing and resistivity calculations.

### 3.2. Effect of Printing Orientation and Parameters on Conductivity

The orientation of printing can influence the porosity of the printed structure or track. When printing conductive materials,

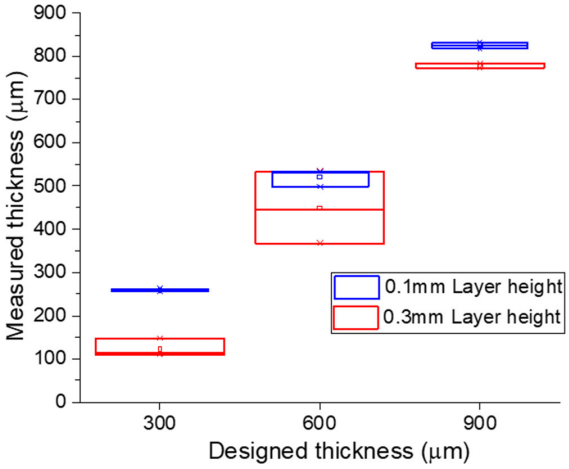


**Figure 5.** Measured thickness of Electrifi tracks printed on the print bed and measured with a profilometer.

the porosity can have a subsequent effect on the conductivity of the track. This effect should be quantified and analyzed for consistent design recommendations and reliable fabrication. **Figure 6** shows the effect of lateral and longitudinal printing orientations on the resistivity of the polymer composite tracks. The connections for all the samples are taken from the ends of the tracks and the resistance is measured longitudinally. For tracks with a 1 mm width, printing laterally presents a decrease in resistivity and higher precision between printed tracks. This is thought to be because of the enhanced connections between the walls of the rectangular track by the connecting infill printed in the lateral direction compared with the longitudinal direction across the small distance. Another factor that could lower the resistivity in the 1 mm lateral infill prints is the added time of the printed Electrifi material under the high temperature of the nozzle. Although this time is in seconds, it remains significant given the thermoplastic's almost instantaneous cooling and solidification as it exits the nozzle. This could keep the printed Electrifi in a molten state for longer, bridging the connections between the rasters more efficiently, and hence giving rise to higher conductivity.

In the 2 mm samples, the resistivity increases with the lateral infill. The continuous deposition of the longitudinal infill tracks gives rise to lower resistivity as the resistance is measured along them. For the 3 mm-wide samples, there is no clear difference in the resistivities of the two different printing orientations. This is due to the creation of equivalent gaps in the tracks in both orientations, contributing to poor connections between the rasters in both longitudinal and lateral infill prints (Figure 6b). A contributing factor as to why the lateral prints of the wider tracks have higher resistivities is the increased time the Electrifi material is in contact with the heated nozzle. This could increase the oxidation of the copper filler in the composite, leading to higher resistivity values.

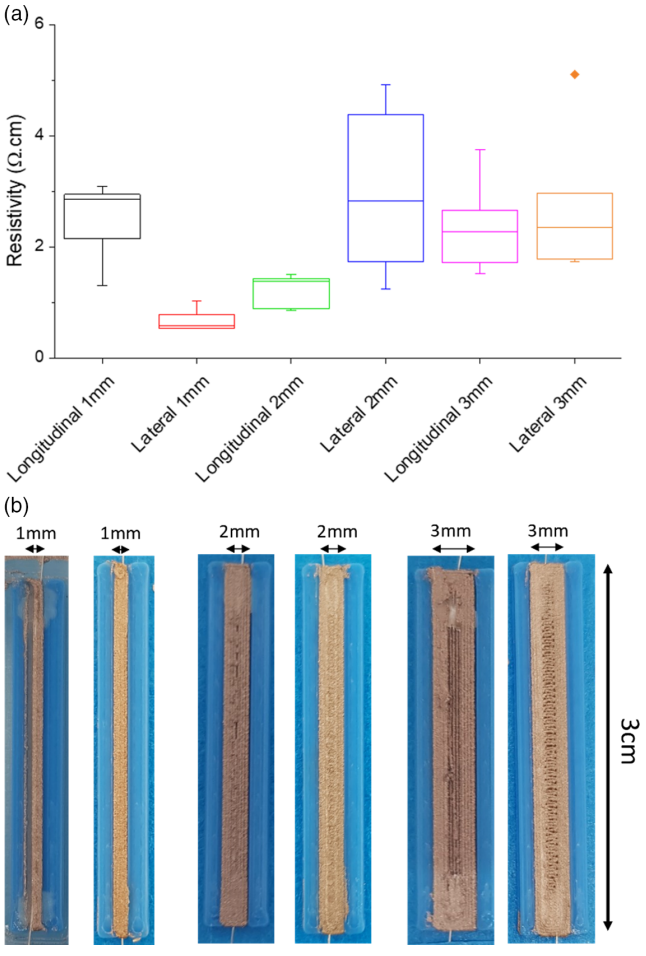


**Figure 6.** Effect of printing orientation on the resistivity of the conductive polymer composites.

It is suggested that with lateral infill printing, as the printer rapidly changes directions, it causes a reduction in the rate of extrusion as it prints the structure. This, therefore, increases the number of voids in the print and might influence the conductivity values based on raster orientation. Printing larger/wider samples is suggested to mitigate this effect. This is observed to be the case between the 2 and 3 mm tracks as the 3 mm-wide tracks offer lower resistivity. However, the lateral printing of the 2 and 3 mm tracks does not improve the resistivity compared with printing longitudinally. This demonstrates that continuous filament flow through the nozzle as well as measuring resistance along the printing direction maintains a significant influence on the resistivity. Moreover, the 1 mm-wide tracks deviate from the trend. This is believed to be because of two reasons: 1) the track width is close to the nozzle diameter, meaning that the effect of distance travelled during extrusion is potentially not very significant in creating gaps, and 2) as the travelled distance is smaller, there is more time at each location for the heated nozzle to be in contact with the printed material, which can better fuse the rasters to give lower resistivity. Overall, there is a trade-off between average printing temperature of the part and continuous filament flow through the nozzle.

### 3.3. Effect of Embedding on Conductivity

For the practical use of 3D-printed smart objects, the printed circuitry will have to be embedded in another insulating thermoplastic. This embedding will undoubtedly influence the electrical characteristics and operating conditions of the conductive tracks. The effect of printing Electrifi with a substrate PLA material is studied and the results are shown in **Figure 7**. The planar-printed tracks are shown in Figure 7a and the vertical 3D ones are shown in Figure 7b. From Figure 7c,d, we can see that for both the planar- and vertical-printed Electrifi interconnects, the resistances are far lower when they are printed alone compared with when they are printed with PLA. The primary reason for this is believed to be the amount of time the Electrifi filament stays in the nozzle during the print. The longer it remains in the nozzle, the more the polymer degrades, leading to higher resistance values of the printed tracks. The higher resistance of the printed tracks, compared with its filament form, is also attributed to the oxidation of the metal filler during the printing process.

The effect of keeping the Electrifi filament in the heated core of the nozzle for longer can also be seen when we study the effect of embedding the conductive tracks in layers of PLA. In Figure 7e, as the number of embedding layers on the top increase, so does the number of substrate PLA layers on the

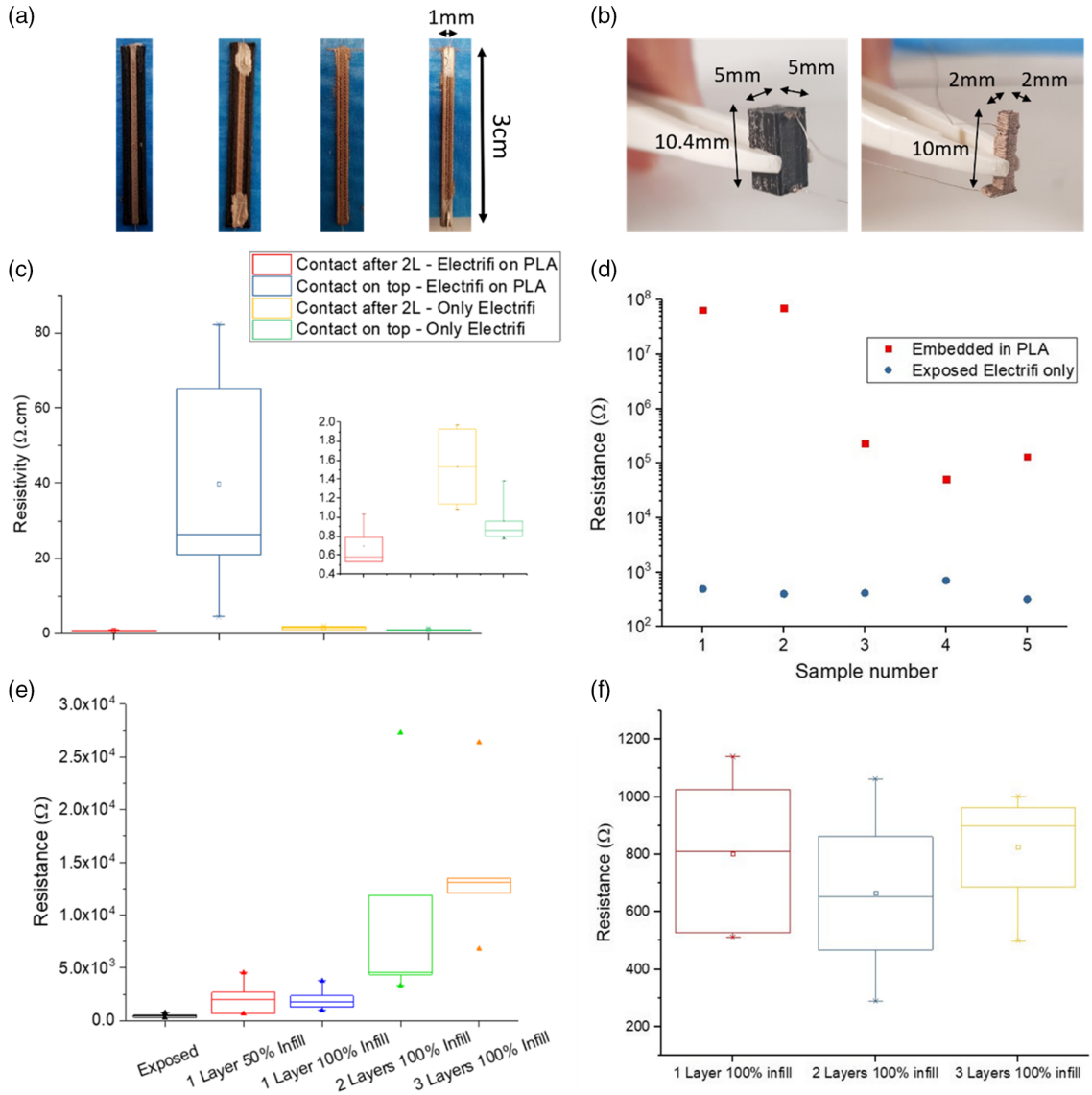


**Figure 7.** Demonstrating the effect of embedding and prolonged time in the heated nozzle on the Electrifi filament. a) Left to right: Electrifi on PLA with embedded connections, Electrifi on PLA with connections on top, only Electrifi with embedded connections, only Electrifi with connections on top. b) Embedded vertical Electrifi track (left) and the exposed one (right). c) The effect of printing Electrifi on PLA on its resistivity and d) the effect of embedding vertical Electrifi interconnects in PLA on their resistance values. The effect of embedding planar Electrifi tracks in PLA on their resistance values is shown for when the e) substrate increases by one layer as the top embedding layer increases by 1 and when the f) substrate has the same/constant thickness as the top embedding layers.

bottom for that structure. This meant that for the track embedded with three PLA layers on the top, three PLA layers were printed on the bottom before the Electrifi was deposited. This was done to place the conductive track in the middle of the structure with equal heat transfer in both the top and bottom directions. This arrangement was also chosen to facilitate similar studies for bendable tracks as equal thicknesses on both sides also bring the conductive track close to the neutral plane and as a result, bending stresses are expected to be low. In Figure 7f, the same numbers of bottom substrate layers are printed before printing the Electrifi for all top embedding layers for comparison. We can see that the longer the Electrifi spends waiting for the bottom PLA layers to print, the higher its resistance value will be (Figure 7e). This is shown as when the substrate thicknesses are equalized, the resistances of the embedded tracks are consistent (Figure 7f). This is also demonstrated in the in Figure S6, Supporting Information, showing the relationship between the resistance of the printed tracks and their location on the print bed when multiple samples are fabricated from one print.

### 3.4. Effect of Embedding on Electrical Performance

In addition to the effect of printing parameters and embedding on the resistance of the printed conductive material, this article

shows the effect of surface area to volume ratio and embedding on its current-carrying capability and electrical performance. **Figure 8** shows the incremental DC current test for the exposed Electrifi tracks on PLA with a track width of 1 mm (Figure 8a), 2 mm (Figure 8b), and 3 mm (Figure 8c). Figure 8d shows a comparison of the power generated at different currents for the three tracks. Results are averaged over five samples and the error bars represent one standard deviation. As expected, due to Joule heating, the measured surface temperature of the printed tracks increases with increasing current and power. The temperature is measured at its highest point in the middle of the track.

The surface temperature at which the tracks fail ranges between 31 and 35 °C for the tracks of different widths. However, there is no clear correlation between the surface temperature at failure and the width of the track. There is a slight increase in the current value at failure as the tracks get wider. A difference is expected due to the wider tracks having more surface area in contact with the ambient air enhancing their cooling. All tracks could only hold their resistance values below 20 mA. The power at which most of the tracks failed varied between 0.08 W and 0.12 W. Despite the limitations, this range is suitable for use with common ICs and electronic components in applications such as readout circuitry for sensors. It is also suitable for use with common communication protocols such as $I^2C$.

**Table 2** shows the electrical suitability and performance of the Electrifi filament used in this study compared with values from a different study and compared with other conductive thermoplastic composites with different base polymers. All the demonstrated operating conditions are for exposed printed tracks. The values shown in the table highlight the maximum operating conditions for conductive composite filaments with different base polymers. Some of the table data are shown in **Figure 9**, highlighting a general correlation between the melting temperature of the base polymer used (or of the composite) and the electrical operating conditions the printed structures can operate under.

In addition to the printed conductive tracks exposed to air at room temperature, the effect of embedding the tracks in layers of insulating PLA is studied. **Figure 10** shows the effect of the number of substrate layers on top of the printed conductive

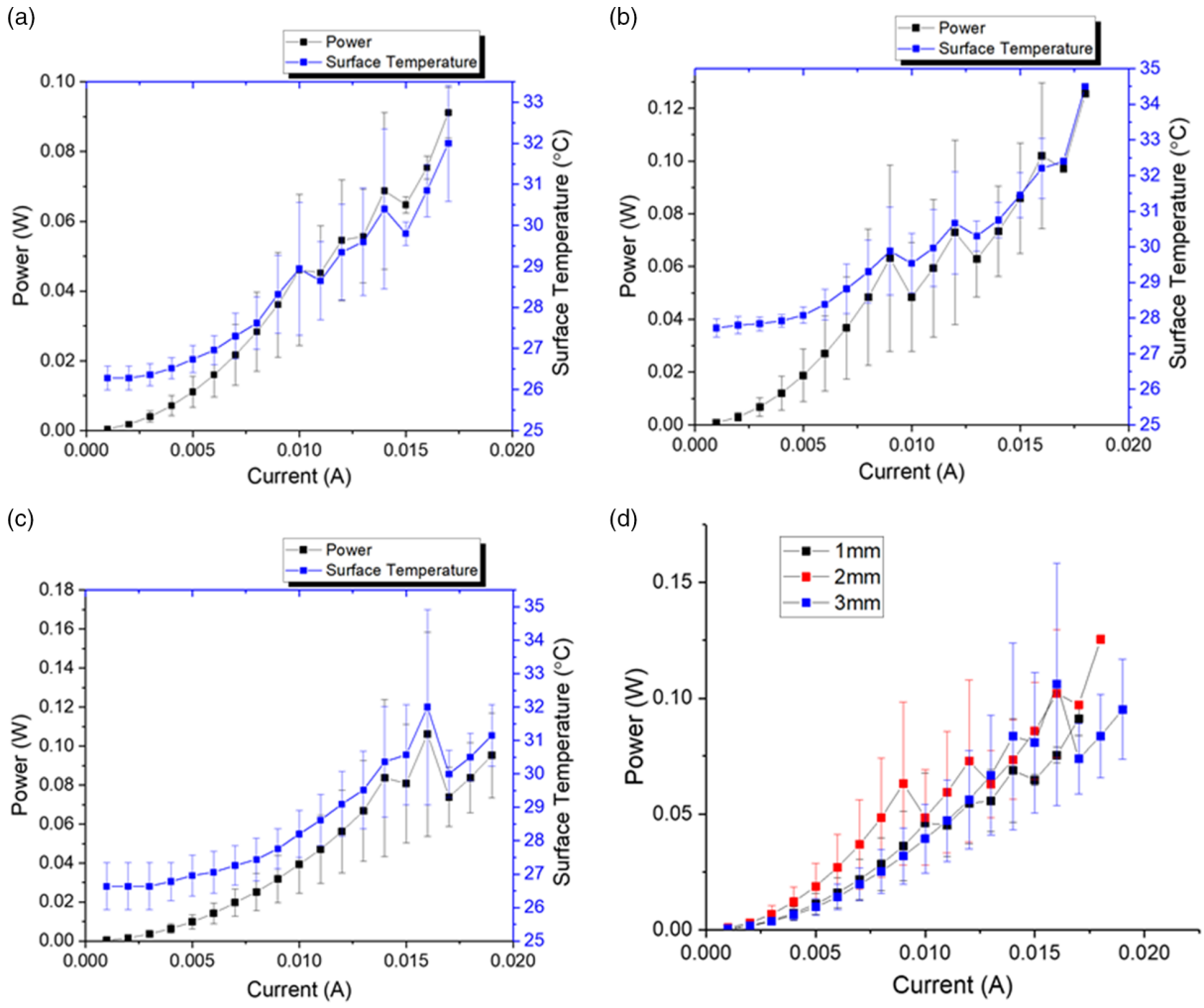


**Figure 8.** DC current test for the Electrifi tracks on PLA with a track width of a) 1 mm, b) 2 mm, and c) 3 mm. d) Comparison of the power generated at different currents for the three tracks. Results are averaged over five samples and the error bars represent one standard deviation.

**Table 2.** Electrical suitability and performance of different base polymers in conductive thermoplastic composites with demonstrated operating conditions in exposed printed tracks.

| Base polymer | Polymer melting temperature/glass transition temperature (melting temperature of composite) [°C] | Max voltage [V] | Max current [A] | Max power [W] | Max temperature [°C] |
|---|---|---|---|---|---|
| Biodegradable polyester[a)] [53] | 60/−60 | 2.2 | 0.18 | 0.4 | 55 |
| PCL[a,b)] [54] | 60/−60 {110} | 1.2 | 0.3 | 0.4 | 110 |
| PLA[c)] [55] | 180/60 | 12 | 0.1 | 1.2 | 50 |
| PP [42] | 160/−20 | 60 | 0.1 | 6 | 125 |
| ABS[d)] [56] | [230]/105 | 24 | 0.3 | 7.2 | 150 |
| PEI[e)] [38] | 340/215 | 10 | 0.5 | 5 | 100 |
| Biodegradable polyester (this work) | 60/−60 | 5.5 | 0.018 | 0.1 | 33 |

[a)]Based on the current density calculation and resistivity value of the printed filament assuming a printed trace with dimensions of 50 mm × 1 mm × 0.5 mm; [b)]Melting point of composite is higher than that of the base polymer alone; [c)]Based on the datasheet recommendations, not a demonstration of the printed filament; [d)]Base polymer in amorphous and has no true melting point, so the value shown is the filament printing temperature; [e)]Filament not tested to maximum operating conditions.

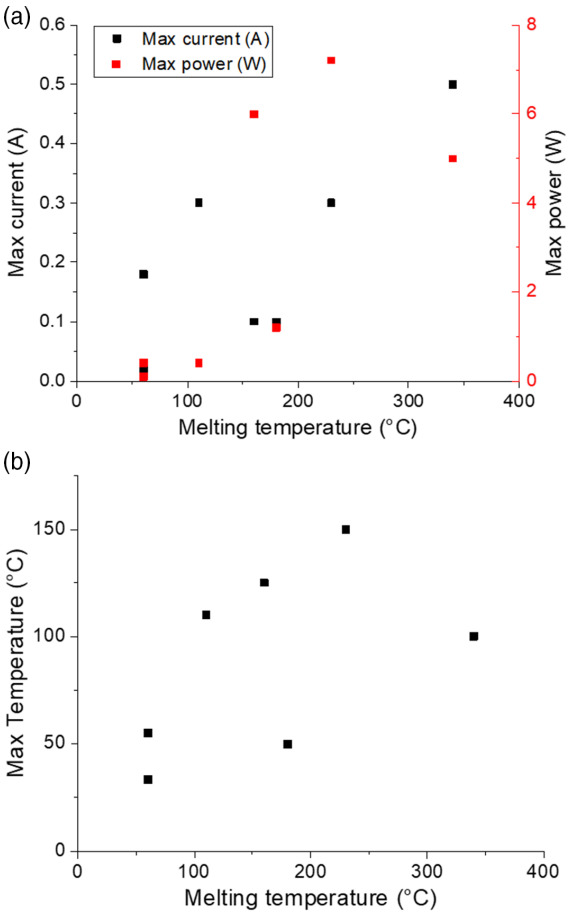


**Figure 9.** The effect of the polymer melting temperature on its electrical performance showing the a) current, power, and b) surface temperature at failure during electrical characterization.

tracks on the durability of the Electrifi composite. This relates to the heat transfer through conduction from the Joule heating at the conductive track through the substrate material to the ambient air. The results show the power generated and the surface temperature of the printed structures as the current incrementally increases. All the conductive tracks are printed on top of the same thickness of PLA to equalize the time the Electrifi filaments remains in the heated nozzle before printing. This is to make the tracks' resistances as consistent as possible. As the current gradually increases, the power generated by the conductive tracks increases. This, therefore, increases the surface temperature of the structures. The exposed tracks can withstand higher currents than the embedded tracks. The results in Figure 10 show the power and surface temperature averaged for five samples with the error bars representing one standard deviation. The exposed tracks can withstand higher currents than the embedded tracks. Once embedded, there is no clear correlation between the number of embedding tracks and the maximum electrical operating conditions.

The results of the incremental current test are shown in **Figure 11**. The average resistance of the exposed tracks is lower than when they are embedded. The high temperature of the nozzle when it is printing the embedding layers might cause slight degradation of the Electrifi composite when they come close to each other. The current at which each of the track fails can be seen to be more closely related to the resistance of the track than the effect from embedding. This is seen in how the exposed tracks can operate at higher currents than the embedded tracks. This trend is not seen as clearly with the generated power at failure. As for the surface temperature, the trend is followed, and we can see that if the printed track has lower resistance, it can withstand higher currents, causing more Joule heating and ending with a higher surface temperature at failure. The higher surface temperature at failure for the exposed tracks can also be attributed to the fact that they are in contact with air and not encapsulated in PLA.

In addition to the resistivity and dimensions of the tracks, the other factors that can influence their electrical performance are the surrounding temperature, the heat transfer coefficient to their surroundings, and their specific heat capacity. The interdependencies of these factors are shown in Equation 3.[54,57]

$$T_x - T_\infty = \frac{J^2 \rho V}{A_{SA} h}\left[1 - \frac{\cos h\left(x\sqrt{\frac{A_{SA}}{V}\times\frac{h}{K}}\right)}{\cos h\left(\frac{L}{2}\sqrt{\frac{A_{SA}}{V}\times\frac{h}{K}}\right)}\right] \quad (3)$$

where $T_x$ is the temperature of the printed track at a point $x$ on the printed track and the temperature of the surrounding air is denoted by $T_\infty$. $J$ is the current density, $\rho$ is the resistivity of the track, $K$ is the thermal conductivity of the track, and $h$ is the heat

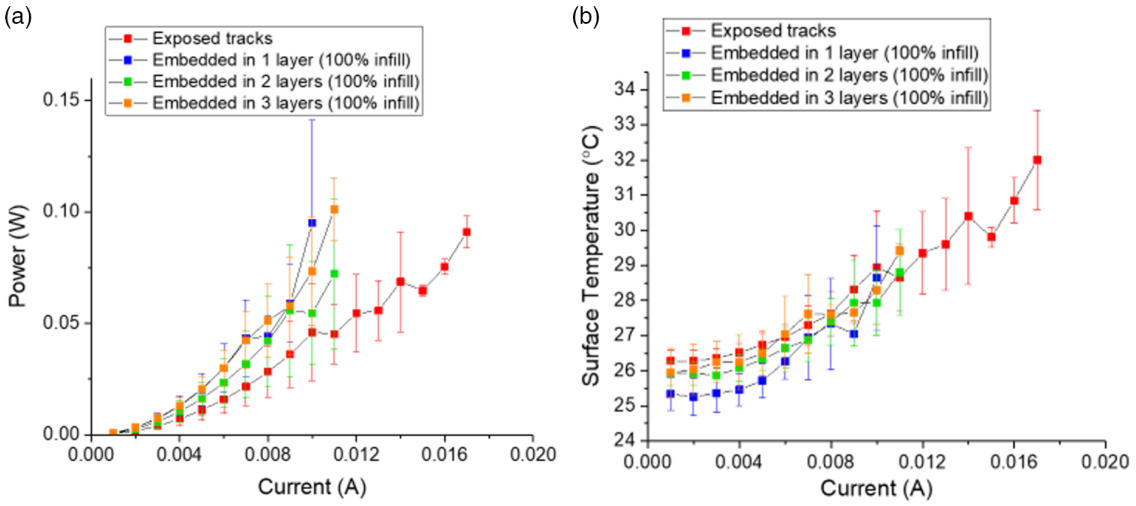


**Figure 10.** The effect of embedding on the electrical performance on the Electrifi printed interconnects with incrementing current. The results shown are for direct comparison of the current versus (a) the power generated, and (b) the surface temperature at failure.

transfer coefficient. For the printed track dimensions, $L$ is the length, $A_{SA}$ is the surface area, and $V$ is the volume. The heat transfer coefficient of the Electrifi filament as well as the thermal conductivity of the embedding PLA (compared with the heat transfer coefficient of ambient air) will affect the current densities of the filament. Generally, we can presume homogenous conduction of heat from the printed conductive tracks to the surroundings.

To remove the effect of different resistances on the electrical performance of the tracks, embedded and exposed tracks with almost equal resistances are printed to isolate the effect of embedding on the values of power, current, and surface temperature at failure. The results are shown in **Figure 12**, where (a) and (b) show the results for tracks with $\approx$500 Ω ($\pm$50 Ω), and Figure 12c,d shows the results for the tracks with $\approx$1 kΩ ($\pm$75 Ω). For the embedded tracks, the measured surface temperature at failure was less than that for the exposed tracks. This is expected as we measure the surface temperature of the embedding PLA compared with the conductive tracks directly. The current and power at which the embedded tracks fail at are less than that for the exposed tracks in all cases. There is no clear trend once the tracks are embedded but more of a binary difference in electrical operating conditions between exposed and embedded tracks. When embedding, the variations can be attributed to the slight difference in resistance, material flow through the nozzle, or fabrication inaccuracies due to the PLA nozzle coming in contact with the printed tracks when embedding. Hence, the internal connections of the fillers in the polymer composite may differ slightly in strength and morphology. The embedding affects the Joule heating transfer through the whole structure causing the conductive tracks to fail at lower currents.

The resistances of the printed tracks change dramatically and somewhat permanently after failure from electrical characterization and degradation. This is shown in Figure S8, Supporting Information, as the difference in track resistance postcharacterization compared with its base resistance before characterization.

Further testing is conducted on a new set of printed conductive tracks with the focus on stability. A fixed current is applied to the printed tracks. The current applied to the conductive tracks is fixed at either 9, 10, or 11 mA, and the time, power, and surface temperature at failure are recorded, as shown in **Figure 13**. Both the embedded tracks with one and three embedding layers fail after 3 min when 9 mA is applied to them. The embedded tracks with two embedding layers do not fail after 90 min of either 9 or 10 mA applied to them. When 11 mA is applied to the tracks with two embedding layers, they fail after $\approx$30 min. The measured tracks with two embedded layers had a slightly lower resistance, allowing them to fail at a slightly higher current value. The small discrepancies in the resistance values of the tracks are attributed to the printing process and the flow of material through the nozzle. Notably, the tracks fail at lower temperatures during the current stress test compared with the incremental current test.

## 4. Realization of a 3D Circuit for Digital Communication

Using the 3D printing setup described in Section 2.1 and the optimal resolution parameters obtained from Section 3.1, a 3D circuit was designed and fabricated to demonstrate the efficacy of using Electrifi as embedded planar and vertical interconnects to send digital data (**Figure 14**). Such a circuit was chosen because this fabrication approach needs to be validated for use in data communication. Sending data is a big part of electromechanical structure design, especially where 3D printing can offer an advantage to traditional PCB use. This is particularly desirable in the production of smart embedded structures for use in applications such as biomedical and remote sensing. Sending digitized sensor reading data through printed interconnects in a 3D circuit is key to realizing 3D-printed smart objects and systems. The $I^2C$ communication protocol is chosen because of its ease of implementation when using multiple sensors in the future. This circuit uses a programmable intelligent computer

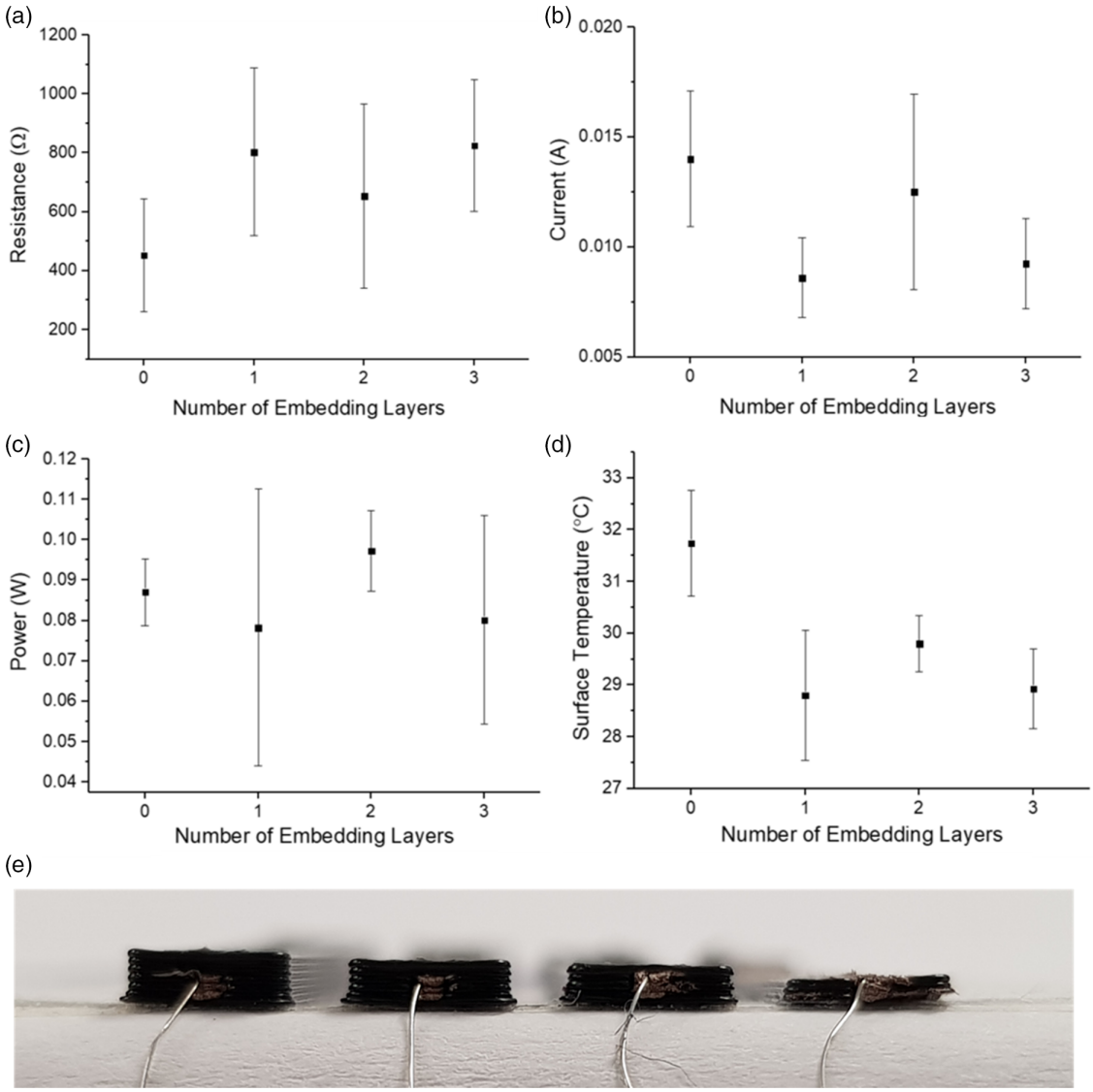


**Figure 11.** The effect of the number of embedding layers on the a) base resistance, b) current, c) power, and d) surface temperature at failure of the Electrifi conductive tracks after DC incremental current testing. e) An image showing the printed tracks embedded in PLA.

(PIC) microcontroller to transfer digital data to an Arduino Due using $I^2C$. A comparison of the performance of a PCB version of the circuit and the 3D-printed version of the circuit is shown in **Figure 15** with the clock and data signals measured using a Keysight Infinii Visionan oscilloscope (Keysight Technologies, Santa Rosa, CA, USA).

In the 3D-printed version of the circuit, after placing the PIC IC, a small volume of conductive silver ink is deposited at the terminals/pins to reduce the contact resistance and ensure good adhesion to the printed Electrifi filament. Figure 14a shows the circuit schematic and Figure 14b shows the CAD design of the 3D-printed version. To reduce the number of electronic components needed in the 3D circuit, the Electrifi's inherent resistivity in the vertical connections (at the Z points in Figure 14b) is used instead of the pull-up resistors. The connections shown in the schematic diagram at points *X*, *Y*, and *Z* are mapped onto the CAD model image.

The application circuit is printed with a planar part and vertical 3D connections. The circuit is shown in Figure 15a. The Arduino is configured with the $I^2C$ address (4) and the PIC microcontroller sends the address, a read bit, and then receives either an acknowledged or not acknowledged bit back from the Arduino. This data transfer sequence is shown for both the PCB version of the circuit and the 3D version of the circuit in Figure 15b.

There is an observed capacitance element to the Electrifi tracks. This capacitance causes a distorted signal shape when the data bit (yellow in the figure) goes from low to high. As the bits are read at the falling edge of the clock signal (green in the figure), it leads to the Arduino not receiving the correct address from the PIC in the case of Electrifi tracks, causing the sequence to not be acknowledged.

In the 3D circuit, the equivalent values of the pull-up resistors created by the planar and vertical Electrifi tracks are 7 MΩ.

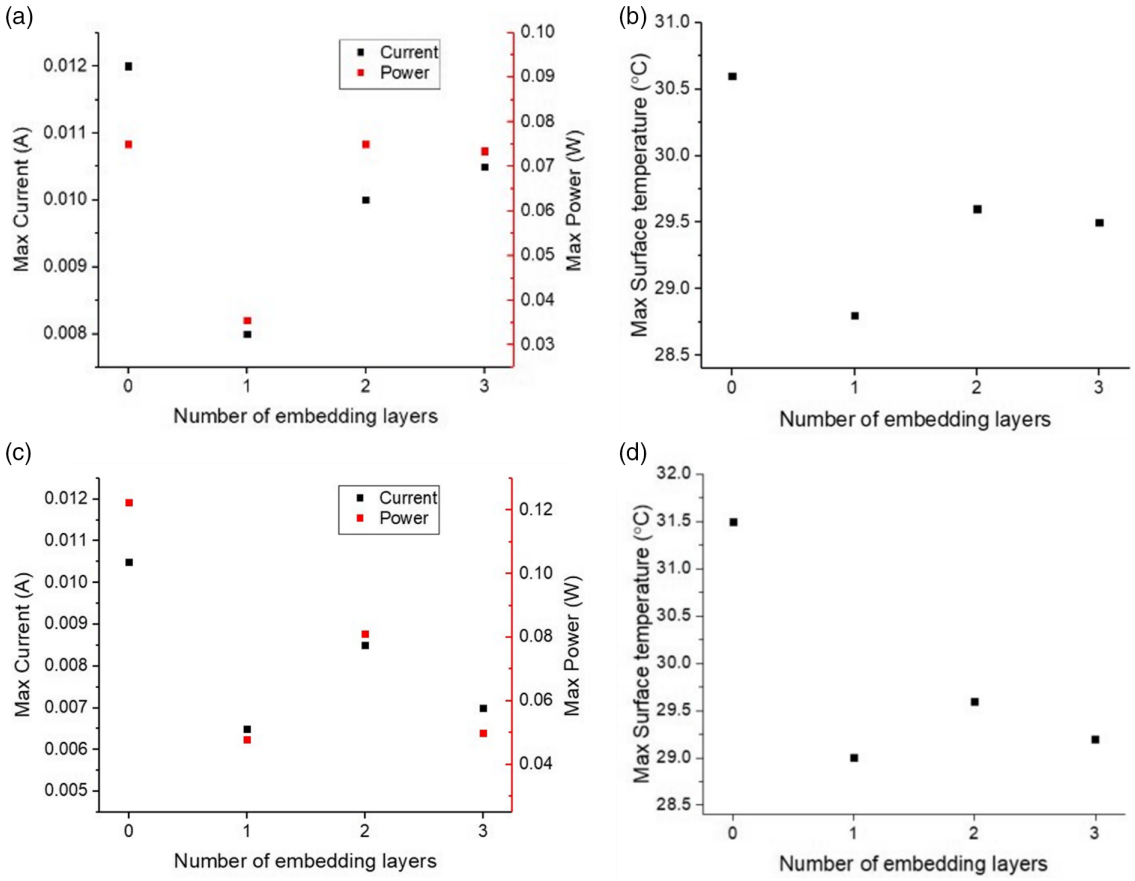


**Figure 12.** The effect of the number of embedding layers on the electrical performance of the Electrifi tracks with equalized resistances. The resistance values are a,b) ≈500 Ω and c,d) ≈1 kΩ.

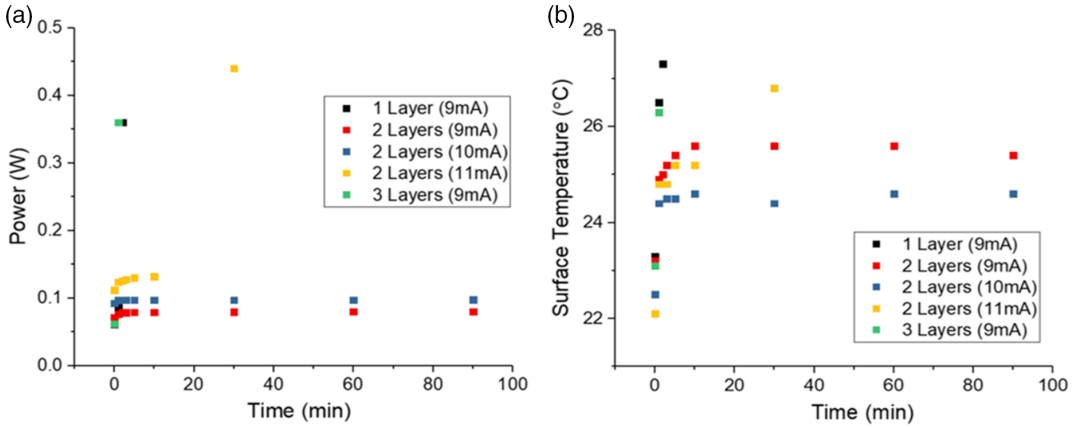


**Figure 13.** The effect of layers of embedding of PLA on the electrical characteristics of the printed Electrifi tracks during a current stress test (constant current applied).

This value is very high compared with the PCB version of the circuit which is 10 kΩ. The larger pull-up resistor value influences the input pin to respond to the voltage change slower. Here, an RC circuit is formed due to the coupling between the line capacitance of the track and the pull-up resistor. When the product of the RC component is large, the capacitance takes a longer amount of time to charge and discharge. This in turn affects the speed and reliability of the pin's change of state. As the serial data line (SDA) value should be stable for the entire high serial clock line (SCL) period, the 3D circuit's instability causes the wrong value (and hence) $I^2C$ address to be registered. Regardless of this issue, we can see that the printed tracks fabricated using this

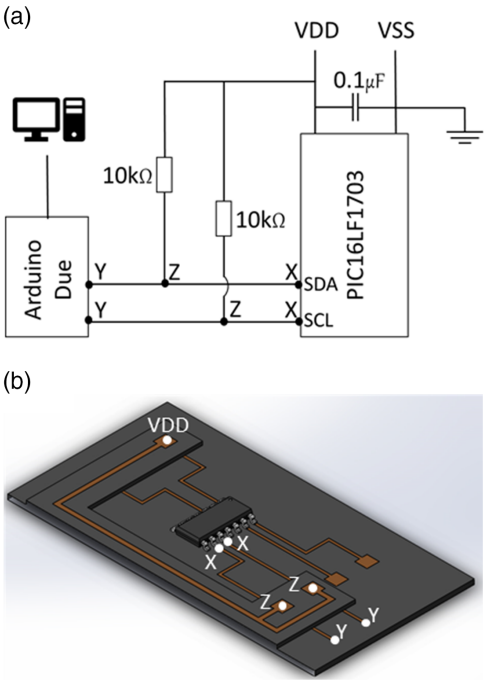


**Figure 14.** a) Schematic diagram of the digital circuit. b) The CAD design showing the 3D version of the circuit.

approach are capable of repeatedly transmitting the data and clock signals through both the planar and vertical connections. Some adjustments such as lowering the pull-up resistor values, or lowering the frequency, could potentially solve this issue, rendering the circuit to be operational.[58] Alternatively, a different communication protocol that relies only on one line (asynchronous), such as universal asynchronous receiver–transmitter (UART), can also be used to avoid the matching of the data and clock lines.

Another similar circuit, fabricated using the same approach with a layer height of 0.15 mm, is shown in **Figure 16**a. The top layer is embedded in PLA to study the influence of embedding on the operation of the 3D circuit. In this case, a larger prime tower size of 40 mm is utilized during printing. This is to ensure that heated Electrifi in the nozzle block is deposited on the prime tower at each layer. This resulted in lower resistivity values for both the planar- and vertical-printed tracks. After printing, the average value for the printed pull-up resistor was 25 kΩ. This is significantly lower than the resistance value in the circuit, as shown in Figure 15. After 1 week, and apparent cooling of the filament at room temperature, as well as drying of the silver paste at the junctions, the average pull-up resistor value decreased to 7 kΩ. This further confirms earlier tests of measuring the printed Electrifi at least 3 days after printing. The resistivity of the Electrifi in the printed circuit is consistent throughout the narrow and wider tracks. It is worth noting that the pull-up resistance values for the first circuit also decreased with time to around 30 kΩ after 2 weeks.

After 1 h of operation, the pull-up resistor value decreased further to 2 kΩ. This is believed to be due to a very small amount of Joule heating in the tracks which could better fuse the filler particles and printed filament in the track. Even with the lowest resistance value, the amount of current passing through the tracks is less than 2 mA and therefore, does not damage the track due to the heating. This confirms the findings in the previous experiments in this article. Moreover, there is no observed negative effect of embedding the top conductive layer in the second 3D circuit.

Despite the lowered pull-up resistor value, the data transmission still exhibited unsuccessful transmission from the microcontroller to the Arduino. As shown in Figure 16b, the data and clock signals could not be pulled all the way down to register logic "0." This is because the pull-up resistor values were too small. This leads to the Arduino not registering the address sent

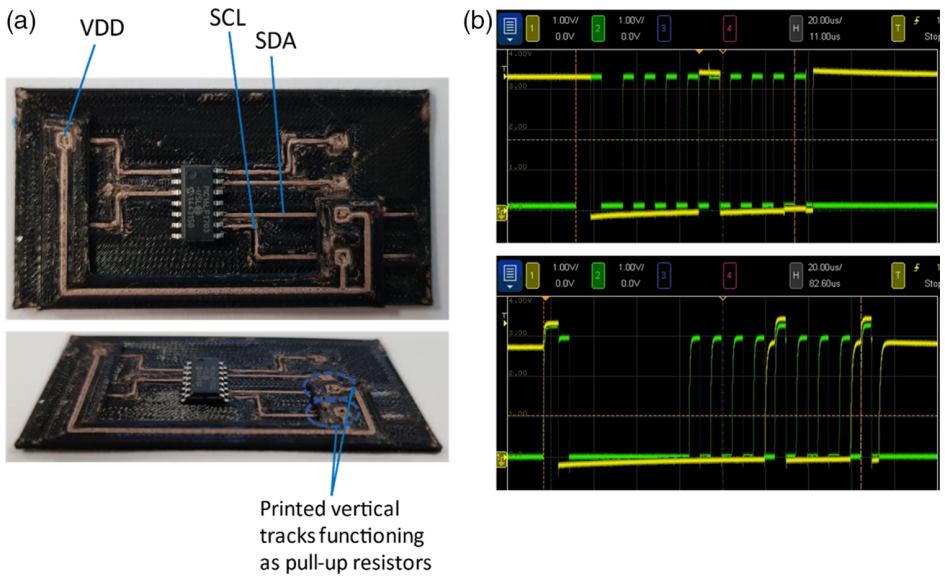


**Figure 15.** a) Images of the printed circuit and 3D interconnections with the PIC microcontroller. b) Oscilloscope readings of the I2C clock and data signals for the PCB (top) and 3D circuit (bottom).

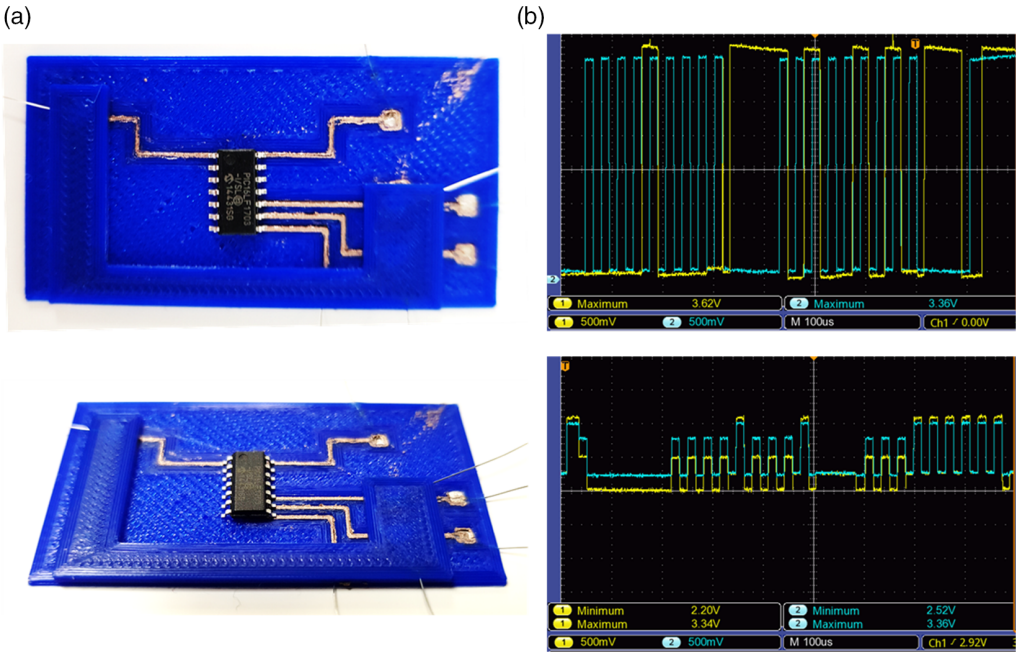


**Figure 16.** a) Images of the second printed circuit and 3D interconnections with the PIC microcontroller and an embedded top layer. b) Oscilloscope readings of the I2C clock (blue) and data (yellow) signals for the PCB (top) and 3D circuit (bottom).

by the PIC microcontroller and the connection is not acknowledged or established. Incorporating embedded SMD resistors in the print process and the fabricated circuit could potentially solve this issue and give way to a fully operable circuit.

Fabricating an exact resistance value of the pull-up resistors in the vertical 3D interconnects is difficult due to the inherent variations in the printing process. Nonetheless, consistent printing of conductive planar and vertical interconnects using the FDM 3D printing approach is achievable and demonstrated here. The printed circuit is capable of digital data transmission and is stable throughout the operation, but the resistance of the printed tracks still needs to be reduced further. Embedding the printed tracks does not impact the electrical performance of the circuit in terms of data transfer.

## 5. Discussion

The bulk conductivity of the filler material as well as the filler wt% and percolation network morphology in a composite play the biggest roles in determining the filament's conductivity. However, its electrical range of operation is also largely determined by its base polymer. The polymer's melting and glass transition temperatures influence the amount of heat they can withstand while still conducting electricity. This, in turn, affects the voltage, frequency, and power conditions they can operate under. Moreover, whether the printed conductor is exposed or embedded in an insulating material will affect the heat transfer and, therefore, the track's electrical operating conditions. The filler material's tendency to get oxidized during the high-temperature FDM extrusion process, as well as the degradation of some polymers, also affect the conductivity of the printed track. All these factors should be considered when designing and fabricating 3D circuits using FDM with embedded conductive polymer composites. While this study focuses on the copper-based Electrifi filament, it provides a basis for investigating the effect of embedding on other composite materials with different filler particles and polymers. These experiments can also be used to electrically evaluate new printable conductive filament materials and study their interactions with different thermoplastic insulators and packaging materials.

The benchmark PCB for an economical technology has a thickness of 37 μm and a width of 100 μm (for 1 oz copper). More advanced PCB technology can produce tracks with a width of 50 μm. In printed electronics, parameters have to be optimized to gain the highest density routing (highest resolution or smallest track widths) with comparable conductivity. With FDM/DIW printing, the resolution of the channel width, with computer numerical control (CNC) micromachining, can normally be achieved to as small as 100 μm (separation between channels of 254 μm). Just using the FDM printer's inherent capabilities (without micromachining), channel widths of around 300−500 μm have been demonstrated and filled with conductive inks. Fully FDM-printed circuits have been demonstrated with track widths of a few millimeters and the recommendations for the pitch between tracks using FDM printers are between 1 and 2 mm. This article realizes smaller track widths and pitch dimensions not previously demonstrated using FDM printing.

## 6. Conclusion

In this article, many elements that effect the fabrication of embedded 3D-printed, planar, and out-of-plane circuits using

FDM are evaluated. The effects of printing parameters on the chosen Electrifi conductive copper-based filament are studied. The effect of lateral and longitudinal printing orientation on the printed tracks' conductivity is also studied. This showed the influence of orientation on 1 mm-wide tracks with lateral infill offering higher conductivity. Wider tracks (2 and 3 mm) were less affected by the infill orientation. A resolution high enough to be compatible with SOIC-packaged ICs is demonstrated using a 0.25 mm nozzle with an average printed track width of 0.67 mm.

Extensive electrical characterization is conducted on exposed and embedded printed tracks to study the effect of embedding on the current-carrying capabilities of the printed tracks and how they were affected due to Joule heating. This was done with both incremental current and constant current stress tests. Exposed tracks performed better than embedded tracks achieving a wider range of operating conditions by failing at higher current values. A 3D circuit with embedded planar and vertical conductive tracks is realized and compared with a PCB with copper tracks. This was done to identify the filament's capability of transmitting digital data signals reliably for future applications in embedded readout circuits. The inherent resistivity of the printed vertical tracks is used to substitute the presence of pull-up resistors in the 3D circuit, thus decreasing the number of electronic components. This article provides a basis for investigating the effect of embedding on multimaterial FDM-printed 3D circuits. Going forward, the artificial intelligence and data-driven approaches could be used for real-time optimization of printer parameters.

## Supporting Information

Supporting Information is available from the Wiley Online Library or from the author.

## Acknowledgements

This work was supported by Engineering and Physical Sciences Research Council through Engineering Fellowship for Growth neuPRINTSKIN (EP/R029644/1), Hetero-print Programme Grant (EP/R03480X/1), and IAA grant (EP/R511705/1).

## Conflict of Interest

The authors declare no conflict of interest.

## Data Availability Statement

Research data are not shared.

## Keywords

additive manufacturing, embedded systems, multimaterial 3D printing, polymer composites, smart objects

Received: May 23, 2021
Revised: July 23, 2021
Published online: September 27, 2021

[1] W. Navaraj, R. Dahiya, *Adv. Intell. Syst.* **2019**, *1*, 1900051.
[2] M. F. Farooqui, M. A. Karimi, K. N. Salama, A. Shamim, *Adv. Mater. Technol.* **2017**, *2*, 1700051.
[3] D. Espalin, D. W. Muse, E. MacDonald, R. B. Wicker, *Int. J. Adv. Manuf. Technol.* **2014**, *72*, 963.
[4] R. Dahiya, D. Akinwande, J. S. Chang, *Proc. IEEE* **2019**, *107*, 2011.
[5] R. Dahiya, N. Yogeswaran, F. Liu, L. Manjakkal, E. Burdet, V. Hayward, H. Jorntell, *Proc. IEEE* **2019**, *107*, 2016.
[6] R. S. Dahiya, M. Valle, in *Robotic Tactile Sensing : Technologies and System*, Springer, New York **2013**, 65–68.
[7] O. Ozioko, P. Karipoth, P. Escobedo, M. Ntagios, A. Pullanchiyodan, R. Dahiya, *Adv. Intell. Syst.* **2021**, 1900145.
[8] W. Gao, Y. Zhang, D. Ramanujan, K. Ramani, Y. Chen, C. B. Williams, C. C. L. Wang, Y. C. Shin, S. Zhang, P. D. Zavattieri, *CAD Comput. Aided Des.* **2015**, *69*, 65.
[9] A. Bandyopadhyay, B. Heer, *Mater. Sci. Eng. R Reports* **2018**, *129*, 1.
[10] O. Ozioko, H. Nassar, R. Dahiya, *IEEE Sens. J.* **2021** *1*.
[11] M. Ntagios, H. Nassar, A. Pullanchiyodan, W. T. Navaraj, R. Dahiya, *Adv. Intell. Syst.* **2019**, 1900080.
[12] R. Khandpur, in *Printed Circuit Boards: Design, Fabrication and Assembly*, McGraw-Hill, New York **2006**, 611–633.
[13] A. Esfandyari, S. Härter, T. Javied, F. Jörg, *Procedia CIRP* **2015**, *26*, 305.
[14] F. Medina, A. Lopes, A. Inamdar, R. Hennessey, J. Palmer, B. Chavez, D. Davis, P. Gallegos, R. Wicker, in *Proc. Int. Solid Freeform Fabrication Symp.*, Austin, Texas, USA **2005**, 39–49.
[15] A. J. Lopes, M. Navarrete, F. Medina, J. A. Palmer, E. MacDonald, R. B. Wicker, in *Proc. Int. Solid Freeform Fabrication Symp.*, Austin, Texas, USA **2006**, 644–655.
[16] J. Palmer, D. Davis, P. Gallegos, P. Yang, B. Chaves, F. Medina, R. Wicker, in *Proc. Int. Solid Freeform Fabrication Symp.*, Austin, Texas, USA **2005**, 476–483.
[17] E. Denava, M. Navarrete, A. Lopes, M. Alawneh, M. Contreras, D. Muse, S. Castillo, E. Macdonald, R. Wicker, in *Proc. Int. Solid Freeform Fabrication Symp.*, Austin, Texas, USA **2008**, 362–369.
[18] A. Joe Lopes, E. MacDonald, R. B. Wicker, *Rapid Prototyp. J.* **2012**, *18*, 129.
[19] Y. Jo, J. Young Kim, S. Jung, B. Yeop Ahn, J. A. Lewis, Y. Choi, S. Jeong, *Nanoscale* **2017**, *9*, 14798.
[20] J. Li, T. Wasley, T. T. Nguyen, V. D. Ta, J. D. Shephard, J. Stringer, P. Smith, E. Esenturk, C. Connaughton, R. Kay, *J. Micromechanics Microengineering* **2016**, *26*, 105005.
[21] S. H. Jang, S. T. Oh, I. H. Lee, H. C. Kim, H. Y. Cho, *Int. J. Precis. Eng. Manuf.* **2015**, *16*, 1361.
[22] E. MacDonald, R. Salas, D. Espalin, M. Perez, E. Aguilera, D. Muse, R. B. Wicker, *IEEE Access* **2014**, *2*, 234.
[23] K. H. Church, H. Tsang, R. Rodriguez, P. Defembaugh, R. Rumpf, in *Proc. IPC Apex Expo*, San Diego, California, USA, February **2013**, 1242–1261.
[24] F. Wasserfall, in *Proc. Int. Solid Freeform Fabrication Symp.*, Austin, Texas, USA **2015**, 180–189.
[25] J. A. Lewis, M. A. Bell, T. A. Busbee, J. E. Minardi, US10462907B2, **2014**.
[26] H. Ota, S. Emaminejad, Y. Gao, A. Zhao, E. Wu, S. Challa, K. Chen, H. M. Fahad, A. K. Jha, D. Kiriya, W. Gao, H. Shiraki, K. Morioka, A. R. Ferguson, K. E. Healy, R. W. Davis, A. Javey, *Adv. Mater. Technol.* **2016**, *1*, 1600013.
[27] H. Nassar, M. Ntagios, W. T. Navaraj, R. Dahiya, *Proc. IEEE Sensors* **2018**, 1, https://doi.org/10.1109/ICSENS.2018.8589625.
[28] T. P. Ketterl, Y. Vega, N. C. Arnal, J. W. I. Stratton, E. A. Rojas-Nastrucci, M. F. Cordoba-Erazo, M. M. Abdin, C. W. Perkowski, P. I. Deffenbaugh, K. H. Church, T. M. Weller, in *IEEE Trans. Microw. Theory Tech.* **2015**, 4382.

[29] K. H. Church, X. Chen, J. M. Goldfarb, C. W. Perkowski, S. Leblanc, presented at *IPC Apex Expo*, Las Vegas, NV, March **2014**.
[30] G. T. Carranza, U. Robles, C. L. Valle, J. J. Gutierrez, R. C. Rumpf, *IEEE Trans. Components, Packag. Manuf. Technol.* **2019**, *9*, 1176.
[31] C. J. Robinson, E. Paso, J. A. Palmer, in *Proc. Int. Solid Freeform Fabrication Symp.*, Austin, Texas, USA **2006**, 60–69.
[32] D. Periard, E. Malone, H. Lipson, in *Proc. Int. Solid Freeform Fabrication Symp.*, Austin, Texas, USA **2007**, 503–512.
[33] J. I. Lipton, D. Cohen, H. Lipson, in *Proc. Int. Solid Freeform Fabrication Symp.*, Austin, Texas, USA **2009**, 711–723.
[34] A. D. Valentine, T. A. Busbee, J. W. Boley, J. R. Raney, A. Chortos, A. Kotikian, J. D. Berrigan, M. F. Durstock, J. A. Lewis, *Adv. Mater.* **2017**, *29*, 1.
[35] S. Bijadi, *M.Sc. Thesis*, *University of Minnesota*, **2014**.
[36] A. Joshi, J. K. Goh, K. E. J. Goh, in *3D 4D Print. Polym. Nanocomposite Mater.* (Eds: K. K. Sadasivuni, K. Deshmukh, M. A. Almaadeed), Elsevier, Amsterdam **2020**, 505–525.
[37] P. F. Flowers, C. Reyes, S. Ye, M. J. Kim, B. J. Wiley, *Addit. Manuf.* **2017**, *18*, 156.
[38] J. M. Gardner, G. Sauti, J. W. Kim, R. J. Cano, R. A. Wincheski, C. J. Stelter, B. W. Grimsley, D. C. Working, E. J. Siochi, *Addit. Manuf.* **2016**, *12*, 38.
[39] NinjaTek | Eel, https://ninjatek.com/eel/, (accessed: November 2020).
[40] B. Krassenstein, *Graphene 3D Lab Launches BlackMagic3D Filament Brand & New Graphene 3D Printing Material*, https://3dprint.com/51502/black-magic-3d-graphene/, (accessed: November 2020).
[41] S. J. Leigh, R. J. Bradley, C. P. Purssell, D. R. Billson, D. A. Hutchins, *PLoS One* **2012**, *7*, 49365.
[42] S. W. Kwok, K. H. H. Goh, Z. D. Tan, S. T. M. Tan, W. W. Tjiu, J. Y. Soh, Z. J. G. Ng, Y. Z. Chan, H. K. Hui, K. E. J. Goh, *Appl. Mater. Today* **2017**, *9*, 167.
[43] *3D Printing Circuit Boards and Components*, https://www.instructables.com/id/3D-Printing-Circuit-Boards-and-Components/, (accessed: November 2020).
[44] K. M. M. Billah, J. L. Coronel, M. C. Halbig, R. B. Wicker, D. Espalin, *IEEE Access* **2019**, *7*, 18799.
[45] Q. Sun, G. M. Rizvi, C. T. Bellehumeur, P. Gu, *Rapid Prototyp. J.* **2008**, *14*, 72.
[46] M. Shojib Hossain, D. Espalin, J. Ramos, M. Perez, R. Wicker, *J. Manuf. Sci. Eng.* **2014**, 136.
[47] B. N. Turner, S. A. Gold, *Rapid Prototyp. J.* **2015**, *21*, 250.
[48] A. Bellini, S. Guceri, M. Bertoldi, *J. Manuf. Sci. Eng.* **2004**, *126*, 237.
[49] M. Yardimci, T. Hattori, S. I. Guceri, S. C. Danforth, *Solid Free. Fabr.*, **1997**.
[50] N. Venkataraman, S. Rangarajan, M. J. Matthewson, B. Harper, A. Safari, S. C. Danforth, G. Wu, N. Langrana, S. Guceri, A. Yardimci, *Rapid Prototyp. J.* **2000**, *6*, 244.
[51] M. Zuza, *Everything about nozzles with a different diameter - Prusa Printers,* https://blog.prusaprinters.org/everything-about-nozzles-with-a-different-diameter_8344/, (accessed: November 2020).
[52] B. George, *Nozzle Sizes — Bob's Project Notebook beta documentation,* http://projects.ttlexceeded.com/3dprinting_nozzle_sizes.html, (accessed: November 2020).
[53] *Revolutionizing Electronics Manufacturing | Multi3D,* https://www.multi3dllc.com/, (accessed: November 2020).
[54] M. A. Cruz, S. Ye, M. J. Kim, C. Reyes, F. Yang, P. F. Flowers, B. J. Wiley, *Part. Part. Syst. Charact.* **2018**, *35*, 1700385.
[55] *Black Magic 3D, B.M. 3D conductive graphene filament,* http://graphenelab.com/blackmagic3d/Filaments/Conductive_Graphene_Filament_216x279.pdf, (accessed: November 2020).
[56] A. Dorigato, V. Moretti, S. Dul, S. H. Unterberger, A. Pegoretti, *Synth. Met.* **2017**, *226*, 7.
[57] A.-T. Chien, S. Cho, Y. Joshi, S. Kumar, *Polymer (Guildf).* **2014**, *55*, 6896.
[58] M. P. Ferrando, *Troubleshooting I2C Bus Protocol,* https://www.ti.com/lit/an/scaa106/scaa106.pdf?ts=1608507709234&ref_url=https%253A%252F%252Fwww.google.com%252F, (accessed: November 2020).